CHINA FOUNDRY Research & Development
Vol. 23 No. 6 November 2026
www.springer.com/41230
https://doi.org/10.1007/s41230-026-5123-4

Thermal modeling of molten metal front in lost foam iron casting

Yun-peng Chang[1], *Feng-jun Li[2, 3], Muhammad Shahbaz Rafique[4], Alex A. Volinsky[5], Meng-nan Liu[2], Jie-qiong Zhang[2], Xiu-qing Li[3], and Feng-zhang Ren[3]

1. School of Intelligent Manufacturing, Luoyang Institute of Science and Technology, Luoyang 471023, Henan, China

2. State Key Laboratory of Intelligent Agricultural Power Equipment, Luoyang 471004, Henan, China

3. Longmen Laboratory, Luoyang 471023, Henan, China

4. School of Mechanical Engineering, Northwestern Polytechnical University, Xi'an 710129, China

5. Department of Mechanical Engineering, University of South Florida, Tampa, FL 33620, USA

Copyright © 2026 Foundry Journal Agency

Abstract: During mold filling in lost foam casting, the molten metal front interacts directly with the polystyrene foam pattern, producing a temperature distribution that fundamentally differs from that in conventional empty-mold casting. Accurate prediction of the temperature distribution at the molten metal front is critical for process optimization and defect control. In this work, a novel physical model was established to characterize the front temperature distribution and interface evolution. Three coupled heat transfer mechanisms are identified as the primary drivers of front temperature variation: (i) heat exchange between the molten metal and the foam pattern, (ii) convective heat transfer within the molten metal, and (iii) heat exchange between the molten metal and the sand mold wall. Based on a radial advancement hypothesis, an interface evolution algorithm was proposed. The heat exchange between the molten metal and the foam pattern is quantified using the latent heat associated with foam gasification. The convective heat transfer within the molten metal is determined by solving the momentum and energy equations, with a specially devised velocity boundary constraint imposed at the filling front, where the normal velocity is specified by a previously established empirical formula. An effective heat transfer coefficient is adopted to simplify the metal-mold heat exchange calculations. The reliability of the developed model was verified through dedicated casting experiments and validated in industrial production. The proposed method provides a reliable and practical tool for predicting filling-related defects and optimizing the process design of lost foam iron castings.

Keywords: lost foam casting; thermal modeling; metal front temperature; cast iron

CLC numbers: TG143/TP391.9 **Document code:** A **Article ID:** 1672-6421(2026)06-838-11

1 Introduction

Lost foam casting offers well-known advantages in dimensional accuracy and production economy[1]. Nevertheless, high defect and scrap rates in complex castings remain major barriers to broader industrial applications[2, 3]. The most prevalent causes of rejection are related to the mold-filling stage. Typical filling-related defects include cold laps, misruns, and inclusions. In some foundries, these filling-stage defects account for approximately 80% of casting rejections[4].

Unlike conventional casting, lost foam casting employs a plastic foam "full mold" rather than an empty cavity, so its process design differs substantially from traditional practice. Foundry technicians commonly rely on trial-and-error methods to optimize lost foam processes[5-8], which are time-consuming, costly, and particularly ineffective for geometrically complex castings.

Several commercial software packages are available for simulating specific aspects of the lost foam casting process[9-12]. These tools primarily address the metal filling sequence, macro-scale temperature distribution, and stress fields, and are used to predict defects such as shrinkage cavities and cracks. However, accurate prediction of defects directly related to the molten metal filling process, such as misruns and cold laps, remains underdeveloped. These limitations highlight

*Feng-jun Li

Ph. D., Professor. Research interests: lost foam casting and non-ferrous alloy processing.

E-mail: ly1688899@163.com

Received: 2025-06-04; Revised: 2025-11-01; Accepted: 2025-12-23

the need for more advanced modeling techniques that can capture the complex interactions between molten metal and the foam pattern during the filling process.

Various computational models have been attempted to simulate the filling process in lost foam casting, given the complex physical and chemical interactions between molten metal and polystyrene foam. For instance, to model the molten metal filling sequence, researchers have proposed different approaches, such as the defined front edge pressure method[13-15], the empirical formula method[16, 17], and the artificial neural network method[18]. To calculate the temperature at the molten metal front, both the decomposition heat method[17] and the heat transfer coefficient method[19] have been introduced. Although these models have been validated under specific process conditions and, when combined with appropriate defect criteria, can effectively predict shrinkage and cracking, robust criteria for predicting filling-related defects in complex iron lost foam castings are still lacking. Since front temperature is the decisive factor in the formation of these defects, developing accurate temperature prediction models is essential.

In view of the heat exchange characteristics of lost foam casting, this study presents a computational method that models the heat exchange between the molten metal at the filling front and the polystyrene foam pattern, the convective heat transfer within the molten metal, and the heat exchange between the molten metal and the sand mold wall. The computational results are experimentally validated using a specially designed test casting and further applied to optimize industrial casting process design.

2 Physical model and algorithms

Lost foam casting is a far more complex process than conventional empty-mold casting, involving coupled heat and mass transfer, fluid flow, chemical reactions, and solidification. The process is also affected by a wide range of parameters, including pattern material and density, vacuum degree, coating permeability, molding sand properties, and pouring temperature. At present, it is impractical to simulate the entire process without appropriate simplifications. Accordingly, the strategy adopted in this work is to construct simplified yet physically representative models for the specific phenomena of interest. The physical model and corresponding algorithms are described in detail below.

2.1 Physical model

The developed physical model targets the calculation of heat transfer and interface evolution at the molten metal front. As illustrated in Fig. 1, when molten metal contacts the polystyrene foam pattern during pouring, rapid decomposition and gasification of the foam occur. A gas gap consequently forms between the advancing metal front and the remaining foam. Under appropriate vacuum conditions, the hot gas trapped in this gap permeates the coating layer and diffuses into the molding sand[14], which in turn accelerates vaporization

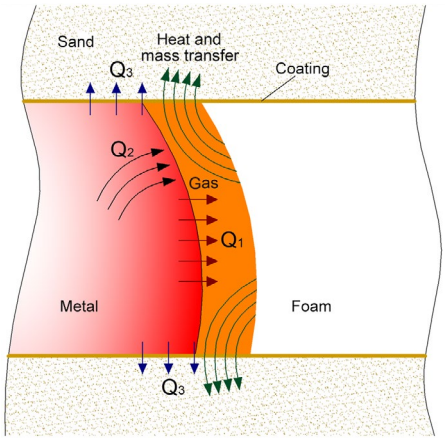


Fig. 1: Schematic of the physical model

and further decomposition of the foam. Under specific process parameters, the gas gap reaches a state of dynamic equilibrium in which the metal filling velocity equals the foam consumption rate.

On this basis, it is proposed that the temperature variation of the molten metal at the filling front is predominantly governed by three coupled heat transfer mechanisms: heat exchange with the polystyrene foam pattern (Q_1), convective heat transfer within the molten metal (Q_2), and heat exchange between the molten metal and the sand mold wall (Q_3).

To reasonably predict the temperature distribution at the molten metal front, the following simplifying assumptions are proposed according to the aforementioned physical mechanisms:

(1) The sprue and ingate dimensions are assumed to provide a sufficient flow rate of liquid metal to establish a pressurized pouring system. In lost foam casting, the ingate should generally not act as a flow choke; otherwise, defects such as sand collapse are likely to occur. This differs notably from conventional empty-mold casting, where the ingate can be intentionally designed as a flow choke.

(2) Each point on the melt-pattern interface is assumed to advance radially along the local surface normal, with the normal velocity as a function of key process parameters: vacuum degree, foam pattern density, pouring temperature, molten metal static head, and coating permeability. This assumption is supported by experimental observations that the foam pattern undergoes radial vaporization when heated by molten metal.

(3) The liquid metal is treated as an incompressible Newtonian fluid, and its flow is governed by the conservation equations of mass, momentum, and energy.

Based on this physical model, the corresponding algorithms for calculating heat transfer and molten metal front evolution are presented in Sections 2.2 and 2.3.

2.2 Heat transfer algorithm

As stated in Section 2.1, the thermal behavior at the molten metal front is dominated by three coupled heat transfer mechanisms. Accordingly, corresponding quantitative calculation methods are developed individually for Q_1, Q_2, and Q_3.

The heat transfer between molten metal and the foam pattern differs fundamentally from that in conventional empty-mold casting. In conventional casting, the metal front contacts air, and interfacial heat transfer is characterized by a heat transfer coefficient. In lost foam casting, the molten metal directly contacts the foam pattern, resulting in intense chilling at the flow front. Although many existing studies and commercial simulation packages still adopt this coefficient-based approach for lost foam casting simulation[17, 19], two major limitations remain: (i) accurate measurement of the interfacial coefficient is highly challenging; (ii) this method does not capture the intrinsic interfacial heat transfer mechanism unique to lost foam casting. To address these limitations, an algorithm based on heat absorption during foam gasification is proposed in this work.

As shown in Fig. 1, when molten metal comes into contact with the foam pattern, heat exchange occurs across the gas gap. The polystyrene pattern absorbs heat from the molten metal, leading to a rapid temperature rise and subsequent endothermic decomposition and vaporization. Accordingly, all heat absorbed by the pattern is sourced from the molten metal. At a given temperature, the heat absorbed by polystyrene, mainly the latent heat of gasification, can be regarded as a material constant obtainable from experimental measurement. The corresponding calculation algorithm is illustrated in Fig. 2. In this schematic, the molten metal front region, bulk molten metal, foam pattern, and sand mold are discretized into independent heat transfer units. The heat exchange between the molten metal front and the foam pattern is treated as a thermal boundary condition. Under a given flow velocity of the molten metal, the specific heat flux across the filling interface is calculated as:

$$q_{out} = d \times L_p \times U \times 10^{-2} \quad (1)$$

where q_{out} is the specific heat flow flux (kJ·s^{-1}·m^{-2}), d is the pattern density (kg·m^{-3}), L_p is the latent heat of gasification of the polystyrene (kJ·kg^{-1}), and U is the normal velocity at the calculation point (cm·s^{-1}).

For the heat transfer between the molten metal and the mold wall, as well as the convective heat transfer within the molten metal, calculation methods analogous to those used in conventional empty-mold casting were adopted, as described in the following section.

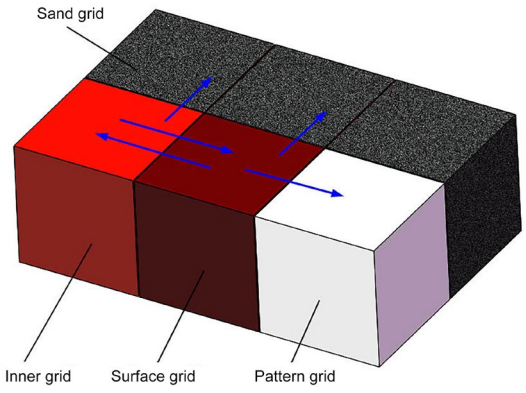


Fig. 2: Schematic of heat transfer algorithm

2.3 Metal front evolution algorithm

To calculate the molten metal front temperature and predict casting defects such as cold laps, it is essential to first characterize the morphological evolution of the molten metal front. The evolution of the molten metal front in lost foam casting differs markedly from that in conventional empty-mold casting. In conventional casting, the molten metal front exhibits a “free surface”, which is dominated by gravity and is typically simulated using the volume of fluid (VOF) method. In lost foam casting, however, gravitational effects are modulated by complex interfacial interactions at the flow front, and the filling morphology is predominantly controlled by the foam gasification mechanism.

The most significant feature of lost foam casting is the presence of a foam pattern in the path of the advancing molten metal front. To reflect this flow hindrance effect, most published studies apply a pressure boundary condition at the molten metal front while still employing the VOF method to simulate the retardation caused by the foam pattern[13-15]. However, this approach yields low accuracy in simulating the front morphology, which in turn reduces the reliability of front temperature calculation and defect prediction.

Based on the radial evolution hypothesis described in Section 2.1, an interface evolution algorithm was developed (Fig. 3). The algorithm assumes that each discrete point on the molten metal front advances outward along the local surface normal, driven thermally, at a locally specific velocity. At each time step, each front point generates a new evolution surface, and the envelope of all such surfaces defines the updated molten metal interface.

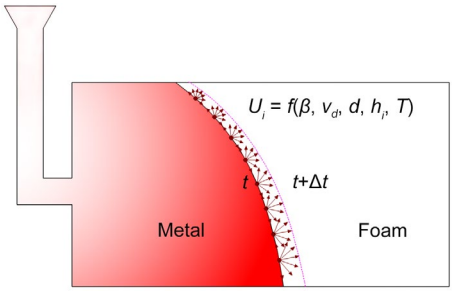


Fig. 3: Schematic of metal front evolution algorithm

The magnitude of the radial advancement velocity at each front point is governed by the key process parameters as follows:

$$U_i = f(\beta, v_d, d, h_i, T) \quad (2)$$

where U_i is the local filling speed (cm·s^{-1}), β is the coating permeability coefficient, v_d is the degree of vacuum (MPa), d is the pattern density (kg·m^{-3}), h_i is the local metallostatic head (cm), and T is the pouring temperature (°C).

The specific empirical correlation in Eq. (2) can be obtained through experimental regression analysis (Section 3). With this algorithm, the lost foam casting filling process was recast as a dynamic calculation of foam pattern recession under thermal action, and convective heat transfer within the molten metal was computed in a dynamically evolving computational domain.

3 Numerical methods and boundary conditions

Based on the physical model and algorithms described above, a numerical simulation framework was developed for the numerical prediction of the lost foam casting process. The overall technical strategy is shown schematically in Fig. 4.

The procedure involves the following steps:

First, the geometric model of the casting was discretized into a structured computational grid. Based on the metal front evolution algorithm, the advancement of the molten metal front was numerically computed at each time step, defining the updated computational domain. Within this domain, the heat exchange terms Q_1 (metal-foam) and Q_3 (metal-mold wall) were calculated using the algorithms in Fig. 2, and applied as thermal boundary conditions. The velocity at the interface, determined from the evolution algorithm, provides the velocity boundary condition. Under these coupled boundary constraints, the convective heat transfer within the molten metal (Q_2) was computed by solving the governing momentum and energy equations. The resulting temperature distribution of the molten metal forms the basis for defect prediction and process optimization.

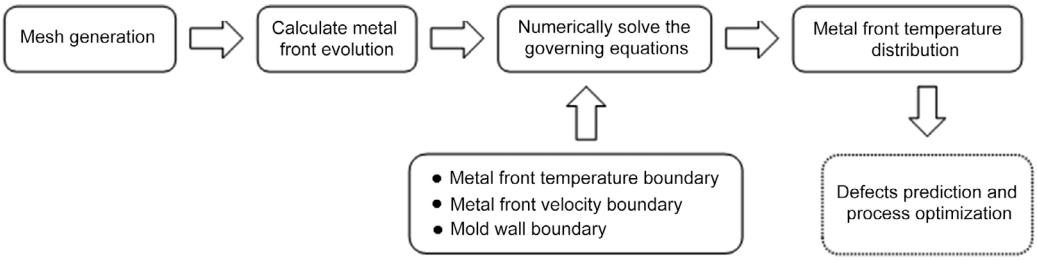


Fig. 4: Overview of numerical simulation methodology

For numerical implementation, the casting geometry was discretized into grids with proper element size (Fig. 5). To accommodate the specific requirements of the interface evolution algorithm, cubic structured grids must be adopted throughout the entire computational domain. In the meshed model, according to the grid classification shown in Fig. 2, grids were categorized into three distinct types: inner molten metal grids, surface grids, and foam pattern grids. Heat transfer among these grid types was calculated using different methods, each tailored to the specific characteristics of the corresponding grid type.

In the numerical approach for the interface advancement algorithm, each surface grid was treated as a discrete point on the molten metal front, which advanced into the surrounding foam pattern. The advancement mode of a surface grid propagating into the surrounding polystyrene foam pattern grids is schematically shown in Fig. 6.

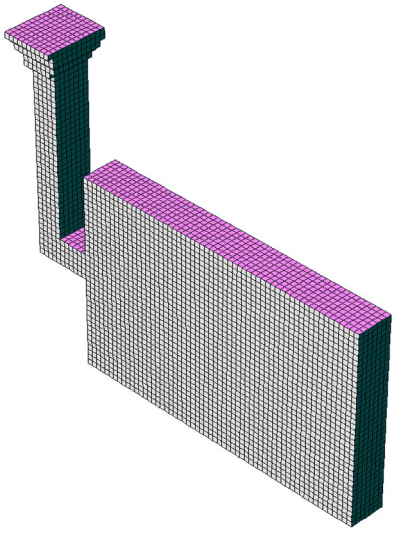


Fig. 5: Computational grid for numerical simulation

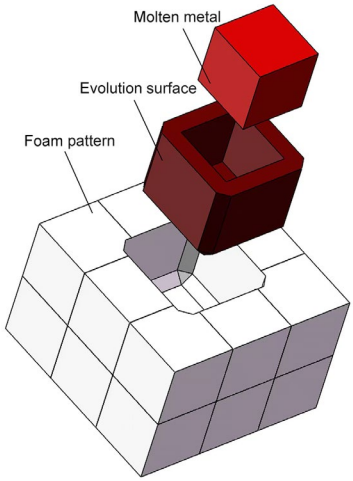


Fig. 6: Schematic of numerical solution for surface grid advancement

The advancement distance of a surface grid propagating into the surrounding polystyrene foam grids within each time step was determined by the local advancement velocity, as follows:

$$\Delta l = U_i \times \Delta t \tag{3}$$

where Δl is the evolution distance (cm), and Δt is the time step (s).

For lost foam iron casting, the filling speed can be calculated using a previously developed empirical equation[16]:

$$U_i = \beta \times (661.967 + 153.96 \times v_d - 0.7632 \times d + 0.8074 \times h_i - 0.940321 \times T + 0.0003397 \times T^2) \tag{4}$$

As time stepping proceeds, once the cumulative evolution distance Δl reaches the critical value for a neighboring grid, that grid is designated as a new surface grid. After each time step, the surface grids are updated to reconstruct the interface and define the updated computational domain. The updated surface grids then continue to propagate into the surrounding grids.

Through interface advancement calculation, a new

computational domain for the molten metal was obtained. The governing equations for the molten metal within the newly defined computational domain are expressed as follows:

$$\frac{\partial}{\partial t}\rho\varphi + \frac{\partial}{\partial x_j}\left(\rho u_j \varphi\right) = \frac{\partial}{\partial x_j}\left(\Gamma_\varphi \frac{\partial \varphi}{\partial x_j}\right) + S_\varphi, \quad j = 1, 2, 3 \quad (5)$$

where φ is a dependent variable, t is time, ρ is the density of molten metal, x_j represents a three-dimensional coordinate component, u_j is a velocity component along the x_j axis, Γ_φ represents the diffusion coefficient, and S_φ is the source term. Equation (5) can be the continuity equation, the Navier-Stokes equation, or the energy balance equation, corresponding to the dependent variable φ being 1, u_j, or T (temperature), respectively. For a certain φ, there are corresponding Γ_φ and S_φ.

The SOLA algorithm was adopted for the numerical solution of these governing equations, with the finite difference method implemented based on the discrete grid illustrated in Fig. 5. The discrete model for interface evolution calculation is fully coupled with the numerical solution of the governing equations. The temperature boundary condition at the melt-pattern interface is treated using Eq. (1). Then, the temperature drop of a surface grid caused by vaporization of the adjacent pattern grid is calculated as follows:

$$\Delta T = -\frac{d \times L_p}{M \times c} \quad (6)$$

where ΔT is the temperature change of the surface grid (°C), L_p is the latent heat of vaporization of the polystyrene (kJ·kg^{-1}), M is the density of molten metal (kg·m^{-3}), and c is the specific heat capacity of molten metal (kJ·kg^{-1}·°C^{-1}).

To define the heat transfer boundary condition between the molten metal and the sand mold wall, a simplified effective heat transfer coefficient is employed[20]:

$$-\lambda \frac{\partial T}{\partial n}\Big|_b = h_f \left(T_{f+} - T_{f-}\right)\Big|_b \quad (7)$$

where $\frac{\partial T}{\partial n}\Big|_b$ is the boundary normal temperature gradient, h_f is the boundary heat transfer coefficient, λ is the thermal conductivity, T_{f+} and T_{f-} are the temperatures on each side of the interface, respectively, and the subscript b denotes the boundary.

To define the velocity boundary condition at the molten metal front, the velocity magnitude was calculated based on Eq. (4). Following the radial displacement assumption induced by melt-foam interaction, the velocity direction was defined as the outward normal to the evolving interface.

The equations presented above were integrated, and a computer code was developed using C++ programming language. Thermophysical properties were obtained from the material database of FT-Star, a casting simulation software package developed by Tsinghua University. Mesh generation and post-processing visualization of the numerical results were also performed on the FT-Star platform.

4 Model validation

4.1 Laboratory validation

To validate the accuracy of the computational model, it is necessary to obtain the actual transient temperature at the molten metal front. However, direct measurement of the instantaneous front temperature during mold filling is extremely difficult in lost foam casting. Since the ultimate filling length is strongly correlated with front temperature (molten metal flow ceases once the front temperature drops below the critical solidification temperature), the measured filling length can be used to indirectly validate the temperature calculation accuracy. Furthermore, filling length is a key metric for evaluating cold laps, misruns, and other mold-filling defects. Accordingly, a spiral test casting was designed for model validation, as shown in Fig. 7. The spiral plate has a cross-sectional width of 20 mm and a thickness of 8 mm, with a total length of 1,900 mm. The ingate cross-section is 10 mm×35 mm. The casting material is HT250 gray cast iron. Key simulation parameters are listed in Table 1. The pouring temperature is 1,500 °C, the foam pattern density is 24 kg·m^{-3}, and the vacuum degree is −0.05 MPa. The mesh element size is 3 mm ×3 mm×3 mm, yielding a total of 4,711,200 elements.

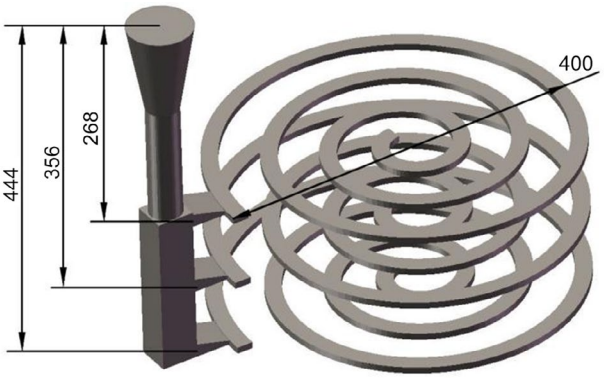


Fig. 7: Casting designed for experimental validation (unit: mm)

The simulated filling sequence and temperature distribution of the molten metal at representative time steps are shown in Figs. 8(a–e). Initially, the upper layer of the spiral plate is filled, as shown in Fig. 8(a), followed sequentially by the middle and bottom layers [Fig. 8(b)]. At the early stage of filling, the upper layer advances farther than the middle and bottom layers. As filling continues, the middle and bottom layers progressively overtake the upper layer [Fig. 8(c)], with the bottom layer ultimately achieving the longest filling distance [Fig. 8(d)]. This phenomenon is mainly attributed to the higher metallostatic head of the bottom layer, which increases the local filling velocity. Figure 8 also illustrates that during the filling process, the front edge of the molten metal experiences a significant chilling effect. This is caused by heat absorption associated with the decomposition of the foam pattern.

For HT250 gray cast iron, the molten metal stops filling when the solid fraction exceeds 0.25[21]. Based on the available data concerning the material used in this experiment, the

Table 1: Experimental parameters and thermophysical data

Parameter	Value
Material: cast iron, wt.%	C: 3.25, Si: 1.95, Mn: 0.9, Cr: 0.28, Cu: 0.35, S: 0.08, P: 0.05.
Latent heat of foam gasification, $kJ \cdot kg^{-1}$	1,003
Density, $g \cdot cm^{-3}$	7.18 (liquid cast iron), 2.8 (sand)
Thermal conductivity, $cal \cdot (s \cdot cm \cdot °C)^{-1}$	0.076 (cast iron), 0.0036 (sand)
Specific heat capacity, $cal \cdot (g \cdot °C)^{-1}$	0.195 (cast iron), 0.18 (sand)
Viscosity, $cm^2 \cdot s^{-1}$	0.04
Interfacial heat transfer coefficient, $cal \cdot (s \cdot cm^2 \cdot °C)^{-1}$	0.0179
Initial sand mold temperature, °C	25
Coating permeability coefficient	1

corresponding critical temperature was determined to be 1,200 °C. Thus, in the simulation, metal flow was terminated at any location where the temperature drops below this critical temperature (1,200 °C). The final simulated filling pattern is shown in Fig. 8(e), and the actual casting produced under these process conditions is shown in Fig. 8(f). A quantitative comparison of simulated and measured filling lengths is given in Table 2.

As shown in Table 2, the maximum discrepancy between simulated and measured filling lengths is approximately 11.8%, which indicates adequate reliability for practical applications such as casting defect prediction and process optimization. Meanwhile, the simulated filling length at the bottom is shorter than the measured value, whereas the opposite is true in the upper layer. A reasonable explanation is that higher metallostatic pressure at the bottom enhances molten metal flowability, so the melt can flow farther than the upper layer after reaching the critical solidification temperature.

4.2 Shop-floor validation

The above-mentioned computational method was applied to optimize the process of an actual industrial casting as a validation case. The casting geometry is shown in Fig. 9. Its overall dimensions are 181 mm×181 mm×238 mm, with a mass of 9.9 kg. The material is HT250 gray cast iron with the following chemical compositions (wt.%): C: 3.23, Si: 1.90, Mn: 0.92, Cr: 0.25, Cu: 0.30, S: 0.06, P: 0.04, balance Fe.

The initial process scheme is displayed in Fig. 10. The pouring temperature is 1,500 °C, the foam pattern density is 25 $kg \cdot m^{-3}$, and the vacuum degree is −0.05 MPa. Subsequently,

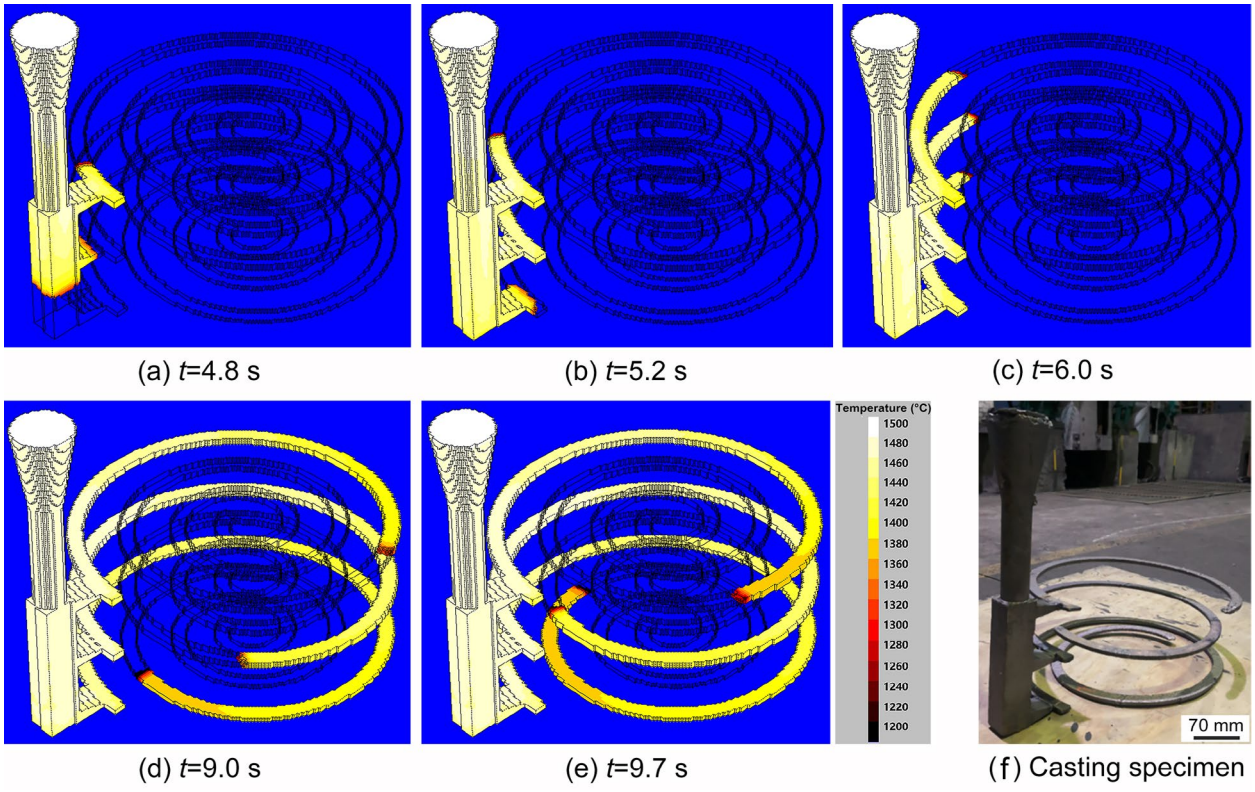


Fig. 8: Filling process simulation at different times (a–e) and casting specimen (f)

Table 2: Comparison of simulated and measured filling lengths

Filling length	Upper	Middle	Bottom
Measured casting length (mm)	907.0	1,231.0	1,677.2
Simulated length (mm)	1,000.9	1,292.3	1,479.8
Difference (%)	10.4	5.0	−11.8

numerical simulation was carried out for this initial process. The thermophysical properties used are those listed in Table 1. The mesh element size is 2.5 mm×2.5 mm×2.5 mm, yielding a total of 7,733,760 elements.

The simulated temperature distribution at representative stages of the filling process is shown in Fig. 11. The molten metal flows through the sprue, runner, and ingate, and then begins to fill the casting. In contrast to conventional empty-mold casting, the molten metal does not wait for the runner to be completely filled before entering the ingate. Instead, it fills the mold in the sequence corresponding to the vaporization of the foam pattern, as shown in Figs. 11(a, b). This phenomenon is consistent with the filling characteristics of the lost foam casting process. Toward the end of filling [Figs. 11(c, d)], low-temperature regions develop near the top of the casting, with temperatures dropping to a minimum of 1,204 °C. In actual production, slight fluctuations in pouring temperature or prolonged pouring time may cause local temperatures to drop below the critical solidification threshold, leading to cold lap defects (Fig. 12). The cold lap defect appears slightly below the top surface of the casting. This is attributed to the "wall attachment" effect, in which vacuum conditions cause the molten metal to adhere to the mold wall and solidify prematurely in that region.

Based on the computational analysis, the process design was optimized as shown in Fig. 13. Four overflow wells were arranged at the top of the casting to divert the chilled molten metal away from the casting body. This modification was intended to improve the temperature distribution in the upper region of the casting and eliminate cold lap defects. The simulation results of the improved process design are shown in Fig. 14. The chilled molten metal is effectively guided into the overflow wells, leading to a remarkable improvement in the temperature distribution within the casting body. Defect-free castings were successfully produced as shown in Fig. 15, which verifies the practical application potential of the proposed model in industrial casting process optimization.

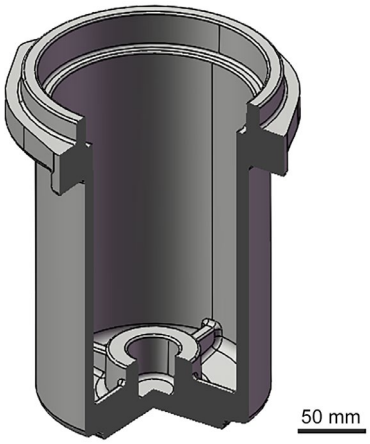


Fig. 9: Industrial casting geometry

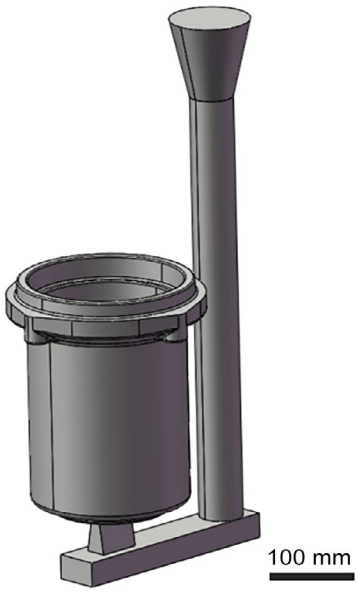


Fig. 10: Initial process design

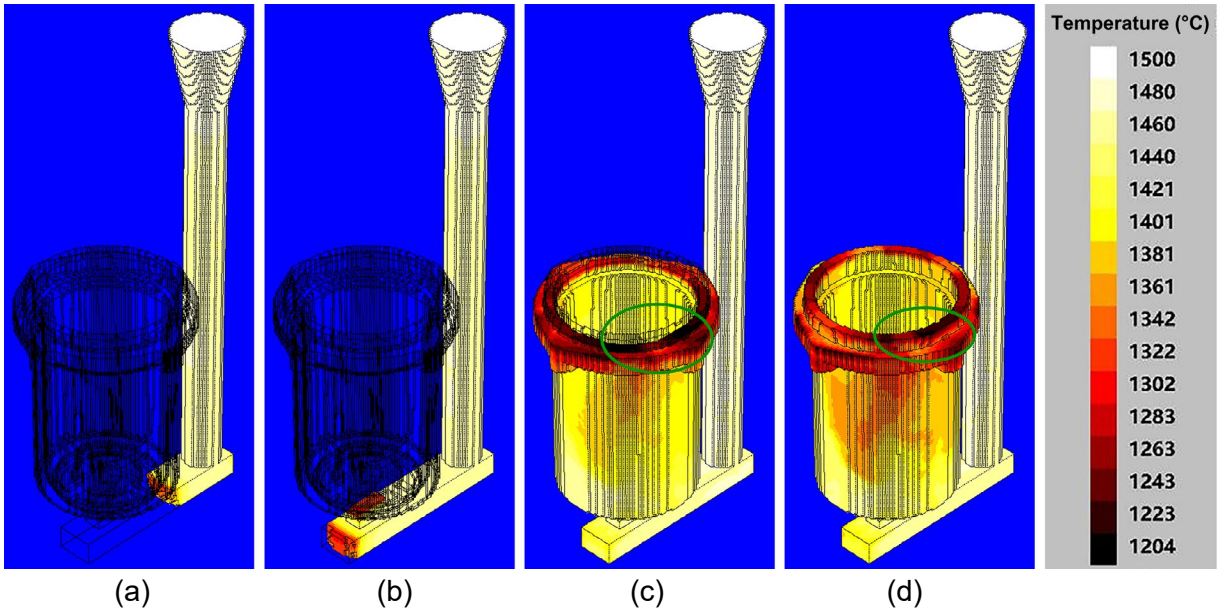


Fig. 11: Temperature distribution simulation of initial process design (a–d)



Fig. 12: Casting defect occurred in the initial process design

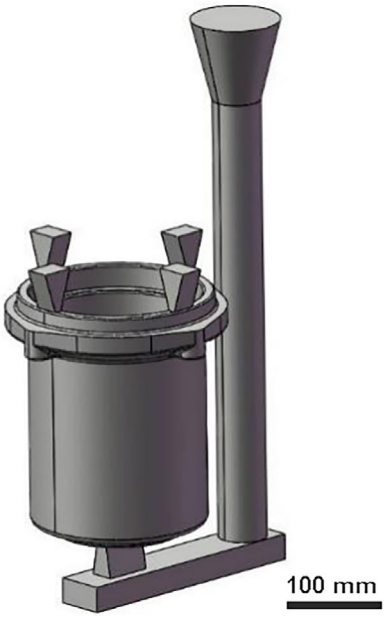


Fig. 13: Optimized process design

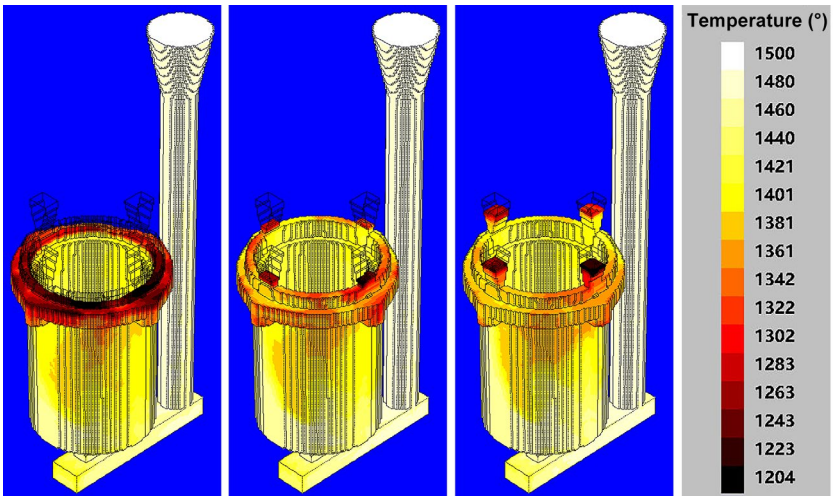


Fig. 14: Temperature distribution simulation of the optimized process design

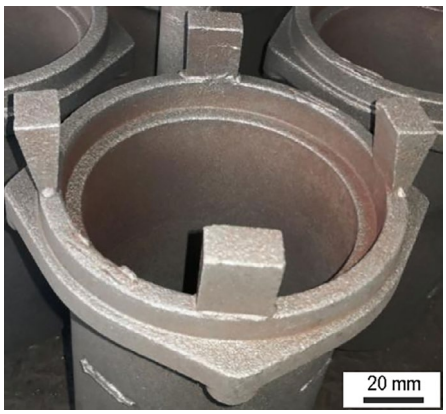


Fig. 15: Defect-free casting produced by using the optimized process

5 Discussion

As described above, significant differences exist in heat transfer and interface evolution between lost foam casting and conventional empty-mold casting, arising from the complex interaction between the molten metal front and the foam pattern. The heat transfer process not only exerts a chilling effect on the molten metal front but also, through the pressure of thermally generated gas, strongly influences the interface evolution morphology. Given these distinctive characteristics and the complexity of the underlying mechanisms, a fully coupled numerical model that simultaneously accounts for thermal effects, fluid flow, and chemical reactions has not yet been realized. Accurate prediction of front temperature and interface evolution therefore remains the central challenge in lost foam casting simulation.

In conventional empty-mold casting, molten metal interface evolution is governed primarily by gravity and atmospheric pressure, and the free surface is typically simulated using the VOF method. In contrast, in lost foam casting, the metal front advances by thermally driven decomposition and displacement of the foam pattern. This thermal action has two defining characteristics: (i) interface evolution is dominated by radial advancement; and (ii) the molten metal front morphology is

jointly influenced by thermally induced gas pressure and gravity.

Concerning the above characteristics, two principal modeling approaches exist for lost foam casting. The first is based on radial evolution: it adopts thermally driven radial expansion as the fundamental mechanism of interface advancement, but typically does not fully account for gravitational effects. The second is based on computational fluid dynamics: it imposes the gas pressure generated by thermal decomposition as a boundary condition at the molten metal front, enabling gravity to be incorporated into the simulation. However, only the average gap pressure can currently be calculated; the transient local pressure at individual front points cannot be accurately quantified, leading to deviations between simulated filling morphology and actual behavior.

To date, mainstream commercial casting simulation software packages worldwide have launched dedicated modules for lost foam casting. As commercial proprietary products, their detailed calculation models and theoretical frameworks have not been publicly disclosed. Nevertheless, their operational workflows and simulation performance can still reflect the fundamental modeling strategies adopted. Both of the approaches described above are adopted in different commercial packages. To further compare the performance of different modeling methods, this study conducts a comparative analysis between the proposed model and two leading commercial casting simulation software packages (Software A and Software B), each equipped with specialized lost foam casting modules.

For comparison purposes, a typical published experimental case concerning molten metal front evolution in lost foam casting was selected[16]. All simulation settings and process parameters were identical to those in the reference experiment, with a pattern density of 13.2 kg·m^{-3}, pouring temperature of 1,400 °C, vacuum degree of –0.047 MPa, and pattern thickness of 20 mm. The mesh element size for all simulations was 2.0 mm×2.0 mm×2.0 mm. The casting geometry, experimental results, and simulated filling morphologies from different models are presented in Figs. 16 and 17.

Software A [Figs. 17(a–c)] yields a filling morphology with distinct radial evolution characteristics, with the molten metal maintaining a vertically symmetric advancing mode. Theoretically, due to gravity, the metal static head in the upper region of the casting is reduced relative to the lower region. Consequently, the foam gasification rate and the resulting filling speed are higher in the lower region, leading to a longer filling length. However, Software A fails to reproduce this gravitational asymmetry.

Software B [Figs. 17(d–f)] exhibits a typical gravity-dominated filling mode similar to conventional empty-mold casting. After entering the ingate, the molten metal flows directly toward the bottom of the casting [Figs. 17(d, e)] and then advances upward layer by layer [Fig. 17(f)]. Although this flow pattern can reflect gravitational effects, it fails to capture the filling characteristics under the hindering effect of the foam pattern, resulting in obvious deviations from actual lost foam casting

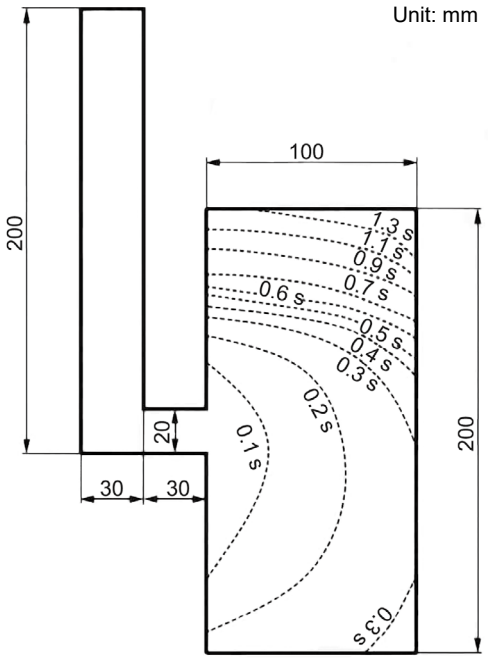


Fig. 16: Evolution of molten metal front in a vertical plate lost foam casting[16]

performance. This discrepancy is especially apparent for castings with large vertical surfaces, thereby limiting its effectiveness for practical applications.

The proposed model treats heat transfer as the dominant mechanism governing interface evolution. While following the fundamental radial advancement mechanism, it simultaneously incorporates gravitational effects through the influence of local metal static head on the front velocity. This coupling between thermally induced pressure effects and gravity enables the model to more faithfully reproduce the temperature distribution and interface evolution pattern at the molten metal front [Figs. 17(g–i)]. As a result, the proposed model can be applied to a broader range of engineering scenarios, simulate more complex lost foam castings, and provide foundry engineers with a reliable tool for predicting filling-related defects and optimizing process design.

6 Conclusions

A novel computational framework for lost foam casting has been developed, comprising a physical model and corresponding numerical algorithms. The following conclusions are drawn:

(1) The temperature at the molten metal front, which critically governs filling-related defect formation, is dominated by three coupled heat transfer mechanisms: heat exchange between the molten metal and the foam pattern (Q_1), convective heat transfer within the molten metal (Q_2), and heat exchange between the molten metal and the sand mold wall (Q_3). Quantitative calculation methods are established for each mode: Q_1 is determined from the latent heat absorbed during foam gasification; Q_2 is derived by solving the momentum and energy equations with appropriate boundary conditions; and Q_3 is simplified using an effective interfacial heat transfer coefficient.

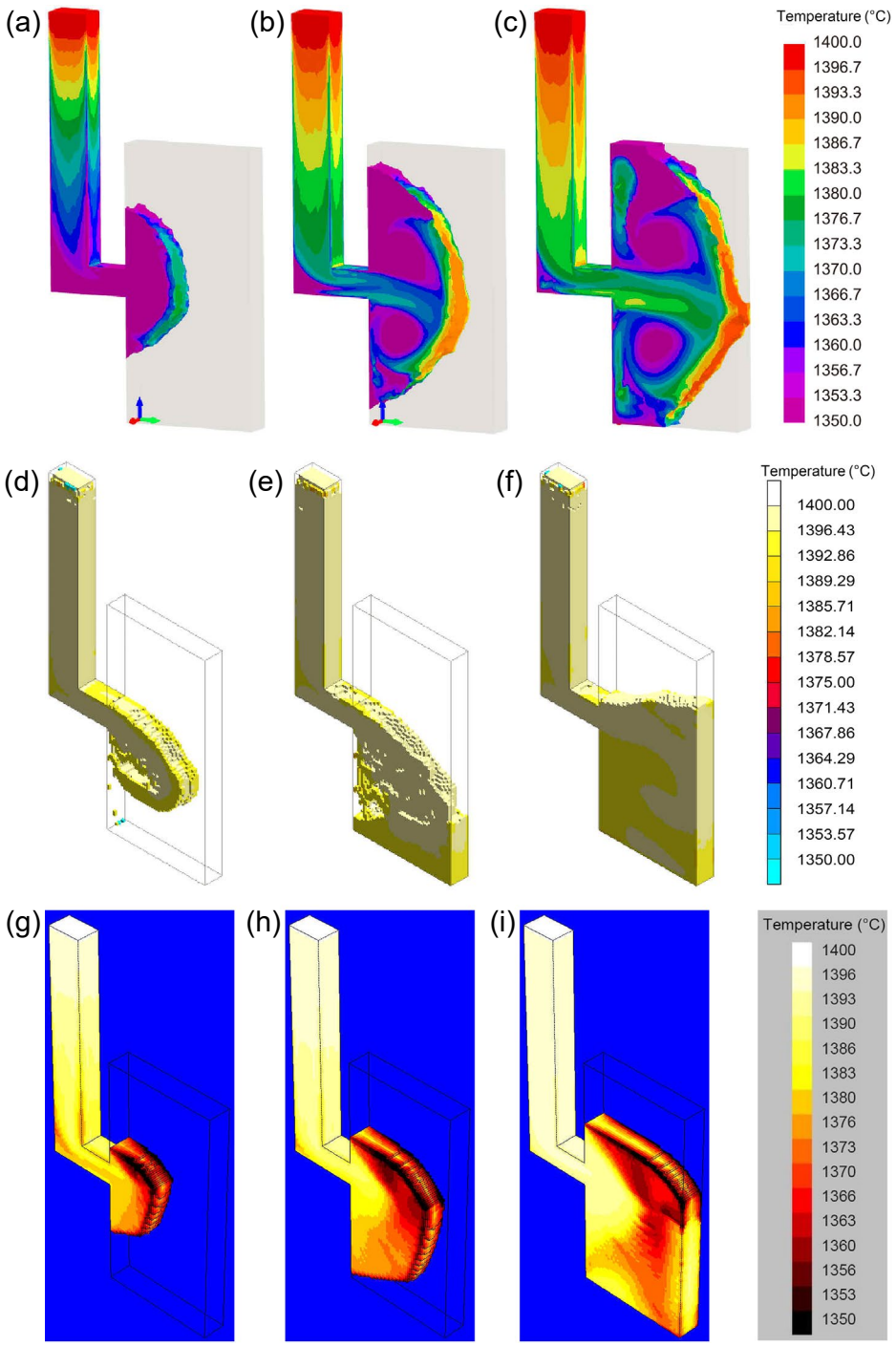


Fig. 17: Comparison of simulated filling morphologies from different software packages: (a–c) Software A; (d–f) Software B; (g–i) proposed model, corresponding to filling percentages of 35%, 55%, and 80%, respectively

(2) Based on the radial advancement hypothesis for the melt-pattern interface, the physical model is coupled with a CFD algorithm to predict the filling pattern and transient temperature distribution at the molten metal front.

(3) Model reliability is verified through a dedicated spiral casting experiment. The maximum discrepancy between simulated and measured filling lengths is approximately 11.8%, which is considered adequate for practical defect prediction and process optimization applications.

(4) The developed method has been successfully applied to industrial production, enabling accurate prediction of cold lap defect locations and guiding the design and optimization of the overflow wells in lost foam iron casting. Defect-free castings have been produced following the optimized process design, confirming the practical utility of the proposed approach.

Acknowledgments

This work was supported by the Frontier Exploration Project of Longmen Laboratory (Grant No. LMQYTSKT001), the National Key R&D Program of China (Grant No. 2020YFB1713500), and the Open Project of the State Key Laboratory of Intelligent Agricultural Power Equipment (Grant No. SKLIAPE 2025022).

Conflict of interest

The authors declare that they have no conflict of interest.

References

[1] Fan Z T, Jiang W M, Liu F C, et al. Status quo and development trend of lost foam casting technology. China Foundry, 2014, 11(4): 296–307.
[2] Bieniewicz K, Reich M, Soraruf N, et al. Improving metal flow in lost foam casting through use of low thermal degradation hot melt adhesives. International Journal of Metalcasting, 2025, 19(1): 34–40.
[3] Jiang W M and Fan Z T. Novel technologies for the lost foam casting process. Frontiers of Mechanical Engineering, 2018, 13(1): 37–47.
[4] Zhang J Q, Li F J, He S W, et al. Research on the testing method of molten metal filling ability in lost foam casting. MW Metal Forming, 2025(1): 122–126. (In Chinese)
[5] Jezierski J, Jureczko M, and Dojka R. The impact of process factors on creating defects, mainly lustrous carbon, during the production of ductile iron using the lost-foam casting (LFC) method. Metals, 2020, 10: 1022.
[6] Li H N, Ji H C, Huang X M, et al. Optimization of defects in the lost foam casting process for fifth wheel coupling shell. International Journal of Metalcasting, 2025. https://doi.org/10.1007/s40962-025-01651-2.
[7] Liang S Y. Process design of ductile iron hub by lost foam casting. Special Casting & Nonferrous Alloys, 2023, 43(4): 574–576. (In Chinese)
[8] Tayal R K, Kumar S, Mondal A, et al. Experimental investigation and parametric optimization of AA6063/AA6351 alloys bimetallic prepared by vacuum-assisted lost foam compound casting process. International Journal of Metalcasting, 2020, 14(1): 243–256.
[9] Huang J, Lin Y X, Chen W P, et al. Numerical analysis of lost foam casting for large-caliber water meter shell. Advances in Mechanical Engineering, 2021, 13(6): 1–14.
[10] Kaliuzhnyi P, Shalevska I, and Shynskyi O. Casting of a steel valve body using lost foam sand casting: Comparison between experimental and simulation results. International Journal of Metalcasting, 2025, 19(4): 2409–2418.
[11] Ma H L and Fu H G. Study on simulation of mold filling and solidification characteristics of hypereutectic high-chromium cast iron by lost foam suspension casting. Metals, 2023, 13(10): 1761.
[12] Sun C, Cao Z Y, Jin Y Z, et al. Numerical simulation of lost-foam casting for key components of A356 aluminum alloy in new energy vehicles. Materials, 2024, 17(10): 2363.
[13] Xie M G, Zhu C A, and Zhou J X. Mold-filling and solidification simulation of grey iron in lost-foam casting. In: Proc. the 5th International Conference on Advanced Design and Manufacturing Engineering. Paris: Atlantis Press, 2015: 387–394. http://doi.org/10.2991/icadme-15.2015.78.
[14] Liu Y, Bakhtiyarov S I, and Overfelt R A. Numerical modeling and experimental verification of mold filling and evolved gas pressure in lost foam casting process. Journal of Materials Science, 2002, 37: 2997–3003.
[15] Charchia A, Rezaeia M, Hossainpourb S, et al. Numerical simulation of heat transfer and fluid flow of molten metal in MMA-St copolymer lost foam casting process. Journal of Materials Processing Technology, 2010, 210: 2071–2080.
[16] Li F J, Shen H F, Liu B C, et al. Molding filling velocity during investment casting. Materials Science and Technology, 2003, 11(3): 225–229. (In Chinese)
[17] Gurdogan O, Huang H, Aakay H U, et al. Mold-filling analysis for ductile iron lost foam castings. AFS Transactions, 1996, 104: 451–459.
[18] Li F J, Shen H F, and Liu B C. Modeling of mold filling and solidification in lost foam casting. Journal of Material Science & Technology, 2003, 19(5): 395–397.
[19] Zhang L Q, Tan W F, and Hu H. Determination of the heat transfer coefficient at the metal-sand mold interface of lost foam casting process. Heat and Mass Transfer, 2016, 52(6): 1131–1138.
[20] Ye J J, Dong H Y, and Xiong S M. Study on a varied grid numerical simulation of mold filling and solidification in casting process. Foundry, 2002, 51(9): 557–560. (In Chinese)
[21] Huang B and Wei B. The shrinkage and feeding behavior of iron castings. Foundry, 1993, 42(9): 14–18. (In Chinese)